JMEPEG (2011) 20:108–113
DOI: 10.1007/s11665-010-9651-z

1059-9495/$19.00

Thermal Expansion and Phase Stability Investigations on Cs-Substituted Nanocrystalline Calcium Hydroxyapatites

Hrudananda Jena, R. Asuvathraman, and K.V. Govindan Kutty

(Submitted June 2, 2009; in revised form March 18, 2010)

The high-temperature phase stability of $Ca_{10-x}Cs_x(PO_4)_6(OH)_2$, ($x$ = 0–3) compositions synthesized by various wet chemical methods was investigated. The thermal expansion property of $Ca_{10}(PO_4)_6(OH)_2$ (abbreviated as CaHAp) and Cs-substituted CaHAp was measured by high-temperature XRD and dilatometry. The average crystallite size of the powders synthesized by wet chemical methods was found to be 10–50 nm range as shown by XRD and TEM. Up to 30 mol% Cs loading was observed to show only the apatite phase by XRD when the apatite powder was nanocrystalline in nature. However, high-temperature stability of the Cs-substituted system is limited to ≤5 mol%. $Cs_3(PO_4)$ is observed to be separated out on heating the material above 773 K for compositions substituted with more than 5 mol% of Cs in the Ca-sublattice. The coefficient of thermal expansion measured by HTXRD is $\alpha_a = 12.42 \times 10^{-6}$ K^{-1}, $\alpha_c = 14.98 \times 10^{-6}$ K^{-1}; and $\alpha_a = 12.62 \times 10^{-6}$ K^{-1}, $\alpha_c = 12.57 \times 10^{-6}$ K^{-1} for CaHAp and $Ca_{9.78}Cs_{0.2}(PO_4)_6(OH)_{1.96}$, respectively, in the temperature range of 298-1083 K. Bulk thermal expansion measurements are seen to be in agreement with the lattice expansion results.

Keywords bulk thermal expansion, Cs-substituted apatite, high-temperature XRD, phase stability

1. Introduction

Hydroxy apatite is a naturally occurring mineral having hexagonal structure with the unit cell formula of $M_5(PO_4)_3(X)$, where M = Ca, Sr, Ba, Pb, Cd and X = OH, Cl, or F (Ref 1, 2). Apatites form solid solutions with various cations (Ref 3) and can immobilize important radioactive elements such as Sr, Cs, and Tc (Ref 4). Apatite minerals form naturally and are stable across a wide range of geologic conditions for hundreds of millions of years (Ref 5-7). Apatites are also used in conditioning the contaminated soil (Ref 8). Apatites are leach resistant in a wide pH range up to 1000 °C (Ref 9, 10). Apatites are also used in the phosphate-induced metal stabilization (PIMS) of contaminants such as Pd, Cd, U, Hg, etc. (Ref 8). Hydroxyapatite has a complicated crystal structure in which the unit cell contains two formula units of $Ca_5(PO_4)_3OH$. In this compound, Ca-ion exists in two different chemical environments, four Ca ions occupy a Ca_I site and other six occupy a structurally distinct Ca_{II} site (Ref 11). Chartier et al. (Ref 12) have carried out the computational studies on Cs immobilization and predicted that the preferential site for Cs and La substitution in $Ca_{10}(PO_4)_6F_2$ apatite to be Ca-I (4f) and Ca-II (6h). The attractive feature of the apatites for nuclear waste immobilization is their ease of preparation at low temperature, which is a prerequisite to avoid volatilization of elements like Cs during the high-temperature chemical processes used for waste matrix preparation. However, application of apatites for nuclear waste management is not extensively studied. Studies related to novel wet chemical synthesis and Cs-loading in hydroxyl apatites was reported in our earlier work (Ref 13). In this study, effect of crystallite size has been investigated on the Cs-incorporation into apatite lattice. The effect of temperature on the phase stability of apatites and Cs-substituted apatites was studied. Further, % thermal expansion of sintered pellets of $Ca_{10-x}Cs_x(PO_4)_6(OH)_2$, x = 0-0.2 compositions were measured by push rod dilatometry and the results were discussed.

Hrudananda Jena, R. Asuvathraman, and **K.V. Govindan Kutty**, Liquid Metals and Structural Chemistry Division, Indira Gandhi Centre for Atomic Research, Kalpakkam 603102, India. Contact e-mails: hnje@igcar.gov.in and kvg@igcar.gov.in.

2. Experimental Procedure

2.1 Sonochemical Reaction

Hydroxyl apatite ($Ca_{10}(PO_4)_6(OH)_2$) was synthesized by using stoichiometric quantities of $Ca(OH)_2$ and $H_2NH_4PO_4$ by co-precipitation followed by ultrasonication at 60-100 °C. Cs-substitutions were carried out by adding stoichiometric amounts of Cs_2CO_3 to $Ca_{10-x}(PO_4)_6(OH)_2$ precipitate and heating at 373-423 K. The compositions ($Ca_{10-x}Cs_x(PO_4)_6(OH)_2$ (x = 0-3) were subsequently heat-treated at various temperatures from 373 to 1323 K, and their phase stability was examined by XRD. Hydrothermal method was also adopted to synthesize the above precursor compositions. The reagents were contained and reacted in a Teflon bowl inside an autoclave at 423 K.

2.2 Characterization of the Powders

The synthesized powders were characterized by XRD (using Siemens D 500 diffractometer or Philips X'Pert Pro MPD system). The powders obtained from all the routes were examined by x-ray powder diffraction, employing a Siemens D-500 powder x-ray diffractometer in the step scan mode using Cu K_α radiation. XRD pattern of the powders heat-treated at various temperatures (298-1123 K) were recorded at 298 K. The heat-treated fine powders were examined by transmission electron microscope (TEM; JEOL 2010, 200 kV) and surface morphology of the oven dried as-prepared powders (consolidated into pellets) and pellets heat-treated at higher temperatures were characterized by scanning electron microscopy (SEM XL 30, Philips, LaB_6 filament and resolution 2 nm). The infrared (IR) spectra of the powders heat-treated at 473, 673, and 1073 K were taken in KBr matrix to identify the presence of hydroxyl groups (Bomem, MB-100 FTIR, resolution 4 cm^{-1}). The powders obtained from decomposition process were examined by TG/DTA (Setaram Instruments, Setsys Evolution 16/18) in order to find out the weight loss characteristics as well as phase transformation, if any, within the programmed temperature range (298-1273 K). The weight loss behavior of the samples was also studied by the temperature-programmed evolved gas analysis in vacuum (10^{-4} Torr) with simultaneous mass spectrometry (EGA-MS) in which the evolved gases were detected in situ by a quadrupole-mass spectrometer (maintained at 10^{-10} Torr). The stoichiometry of the compositions was confirmed by wet chemical methods. Cs and Ca compositions were detected by atomic absorption spectroscopy (AAS) methods. The Ca/P ratio was found to be 5.0:3 in case of undoped apatite. The Cs-doped composition shows a Ca/P ratio of 4.89:3 and Cs is 0.2 mol in case of $Ca_{9.78}Cs_{0.2}(PO_4)_6(OH)_{1.96}$. The estimated values are within the error of ±5%.

2.3 Crystallite Size Measurement by Using Scherrer Formula

The crystallite size of the powders were measured by using Scherrer formula (Ref 14, 15), $t = 0.9\lambda/D \cos\theta$, where t = crystallite size, $B = (\beta^2 - B^2)^{1/2}$, β = sample broadening, and B = instrumental broadening in radians. The instrumental broadening was measured by using NBS Si as standard. λ is the wave length of x-radiation (Cu K_α). The crystallite size measured by XRD is compared with particle size measured by TEM and SEM.

2.4 Thermal Expansion Measurements by XRD and Dilatometry

The thermal expansion behavior of the CaHAp and Cs-substituted analogs were investigated by high-temperature XRD (HTXRD) and dilatometry. The HTXRD measurements were carried out by using the HTK-16 module of Philips X'Pert Pro MPD system. The powder samples were mixed with Pt powder (1:5 = Pt:CaHAp wt. ratio) as internal standard for temperature correction. The fine powders were mounted on the tantalum strip (sample carrier) that was resistively heated at programmed rates. The sample temperature was monitored with a thermocouple spot welded to the rear of the sample carrier strip. All measurements were carried out in a vacuum of about 10^{-5} Torr. The XRD patterns of the samples recorded at room temperatures, and then the temperature was increased in steps of 100-1173 K. The lattice parameters were obtained from the XRD data at each temperature. The lattice parameters, l, were fitted against temperature (in Kelvin) to the polynomial expression: $l = x + yT + zT^2$. The average axial expansion coefficient, α_l, between the temperatures, T_1 and T_2, was calculated by the equation, $\alpha_l = (l_2 - l_1)/(l_1(T_2 - T_1))$, where l_1 and l_2 are the lattice parameters at temperatures T_1 and T_2, respectively. Similarly, the average volume expansion coefficient, α_v, was also calculated. The average linear expansion coefficient, $\bar{\alpha}$, was calculated by the following expression: $\bar{\alpha} = \alpha_v/3 = (2\alpha_a + \alpha_c)/3$. Bulk thermal expansion measurements were carried out on sintered pellets using a home-built push rod dilatometer (Ref 16).

3. Results and Discussion

3.1 Solid Solution Formation and Phase Stability

Wet chemical methods yielded nanocrystalline (10-50 nm) phase pure powders of $Ca_{10}(PO_4)_6(OH)_2$ as evident from the XRD patterns shown in Fig. 1. The nanocrystalline nature of the powders was further confirmed by TEM and SEM examinations of the samples. The TEM micrograph of $Ca_{10}(PO_4)_6(OH)_2$ powders show an average size distribution of 10-50 nm as shown in Fig. 2(a), and the selected area electron diffraction (SAED) pattern of the powders show ring patterns (Fig. 2b), indicating nanocrystalline nature of the powders. The TEM micrograph of the as-prepared powders shows needle-shaped structures, which was also observed by various other investigators (Ref 17, 18). The SEM of the pure $Ca_{10}(PO_4)_6(OH)_2$ shows compact relatively pore free microstructure (Fig. 3a) on heat-treatment at 1073 K. The SEM (Fig. 3b) of 2 mol% Cs-substituted composition does not show flaky structure indicating the incorporation of Cs into the apatite matrix and 5 mol% Cs-substituted hydroxyl apatite compositions show a flaky structure (Fig. 3c).

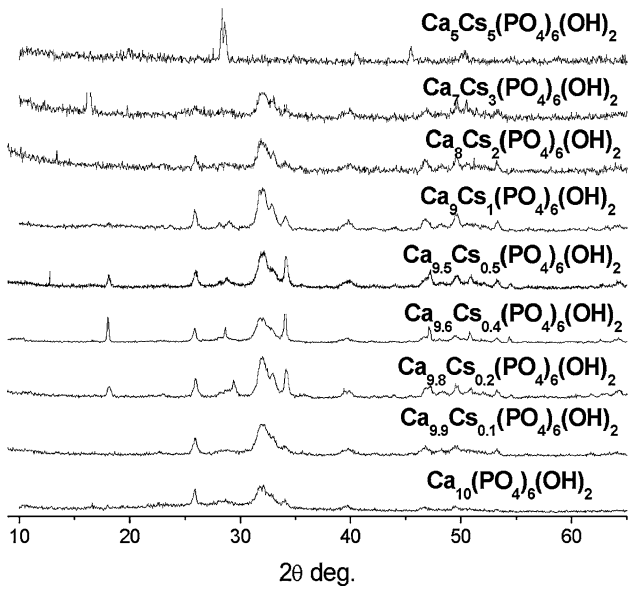

Fig. 1 XRD pattern of as-prepared oven dried $Ca_{10-x}Cs_x(PO_4)_6(OH)_2$, x = 1-5

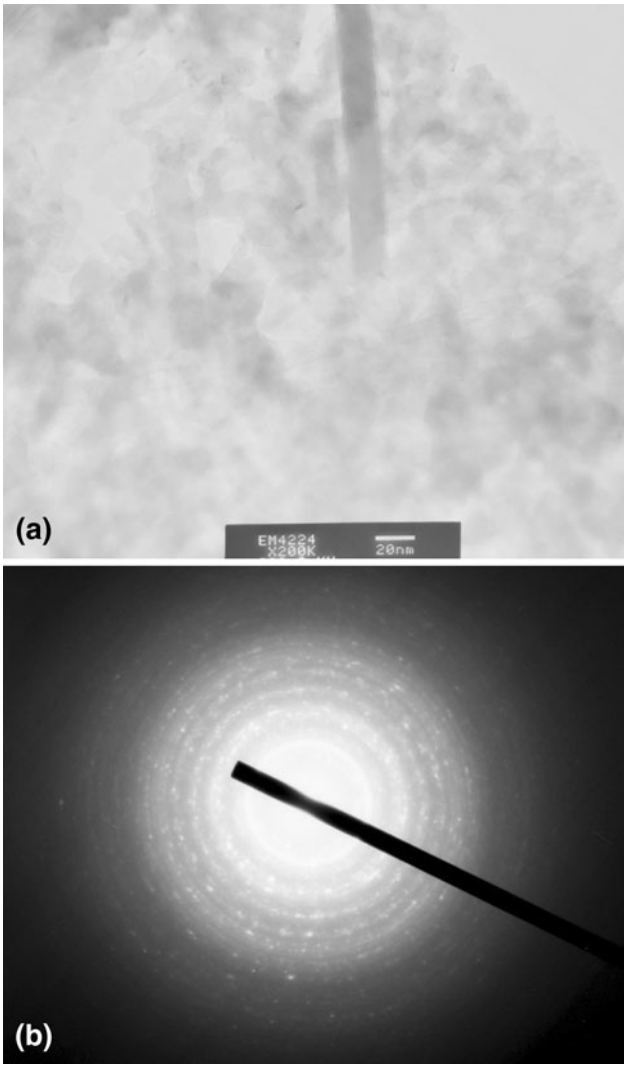

Fig. 2 (a) TEM micrograph of $Ca_{10}(PO_4)_6(OH)_2$ showing needle-shaped structures (average size 10-50 nm). (b) Selected area electron diffraction (SAED) pattern of as-prepared $Ca_{10}(PO_4)_6(OH)_2$, showing ring patterns

Further, 30 mol% (i.e., Cs/(Cs + Ca) = 0.3) of Cs-substitution into Ca-sublattice yielded single nanocrystalline CaHAp phases as shown in Fig. 1. Also, 50 mol% (i.e., Cs/(Cs + Ca) = 0.5) of Cs-substitution yielded Cs_3PO_4 (cubic system, a = 8.83 Å) as the major phase without heat-treatment of the precursor powders as shown in Fig. 1. However, on heat-treatment above 773 K, Cs-substituted compositions (i.e., $Ca_{10-x}Cs_x(PO_4)_6(OH)_2$, $x \geq 0.5$) decomposed to bi- or tri-phasic mixtures of $Ca_{10-x}Cs_x$HAp, Cs_3PO_4 and CaO, whereas $Ca_{10}(PO_4)_6(OH)_2$ composition is stable up to 1423 K as shown in Fig. 4.

The phase instability of $Ca_{10-x}Cs_x(PO_4)_6(OH)_{2-\delta}$, $x \geq 0.5$ compositions and occurrence of Cs_3PO_4 as a separate phase may be attributed to the ionic radius mismatch. The ionic radius of Cs^+, i.e., $\left(r^{VII}_{Cs^+} = 1.71\ \text{Å}, r^{IX}_{Cs^+} = 1.78\ \text{Å}\right)$ is larger compared to that of Ca^{2+} $\left(r^{VII}_{Ca^{2+}} = 1.06\ \text{Å}, r^{IX}_{Ca^{2+}} = 1.18\ \text{Å}\right)$ (Ref 19) in the Cs-doped CaHAp lattice. A computational study of Cs immobilization in $Ca_{10}(PO_4)_6F_2$ apatite by Chartier et al. (Ref 12) reported size constraints leads to the instability of

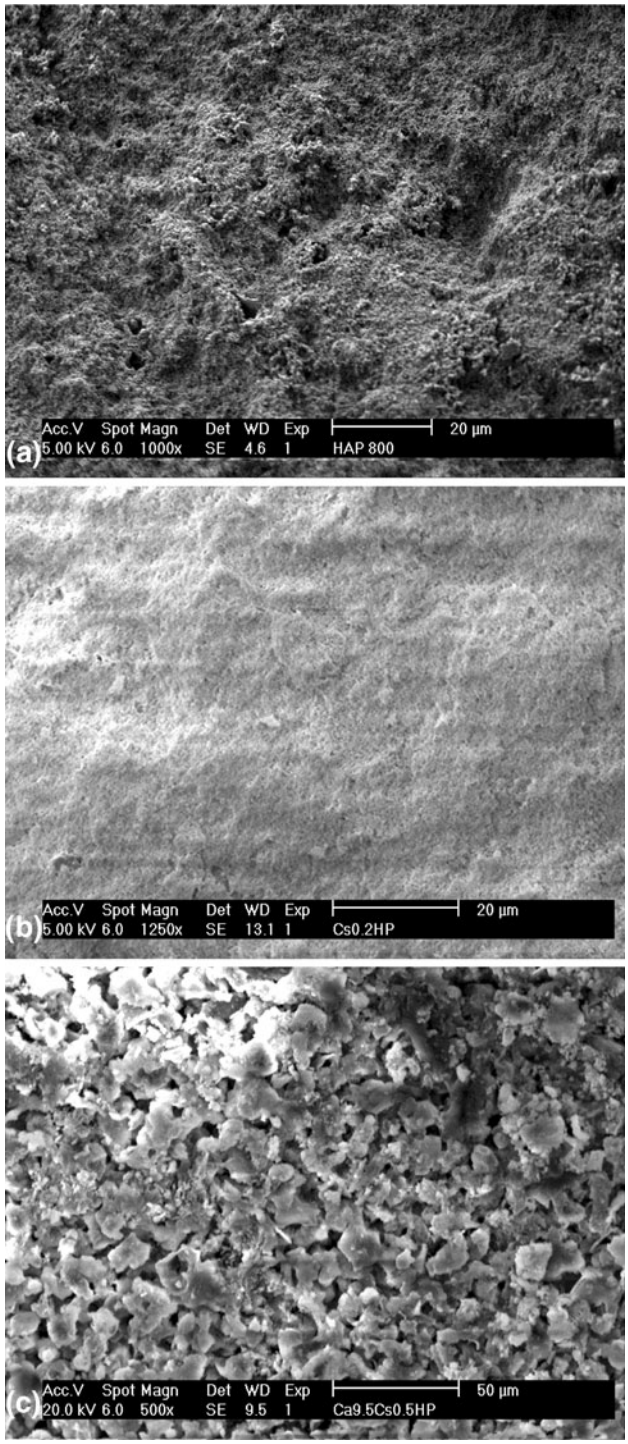

Fig. 3 (a) SEM micrograph of $Ca_{10}(PO_4)_6(OH)_2$ composition heat-treated at 1073 K. (b) SEM micrograph of $Ca_{9.8}Cs_{0.2}(PO_4)_6(OH)_2$ composition. (c) SEM micrograph of $Ca_{9.5}Cs_{0.5}(PO_4)_6(OH)_2$ composition

the Cs-loaded apatite matrix. Hence, very limited amount of Cs-substitution is recommended in the apatite matrix. To attain charge neutrality, stoichiometric amounts of OH^- ions are removed from the lattice forming hydroxyl defects. Crystallographically apatite has 10 Ca-atoms per unit cell, which are arranged in two different coordination spheres such as Ca_I-O_9 and Ca_{II}-O_6X ($X = OH^-$) polyhedra (Fig. 5). Ca_{II}-O_6(OH)

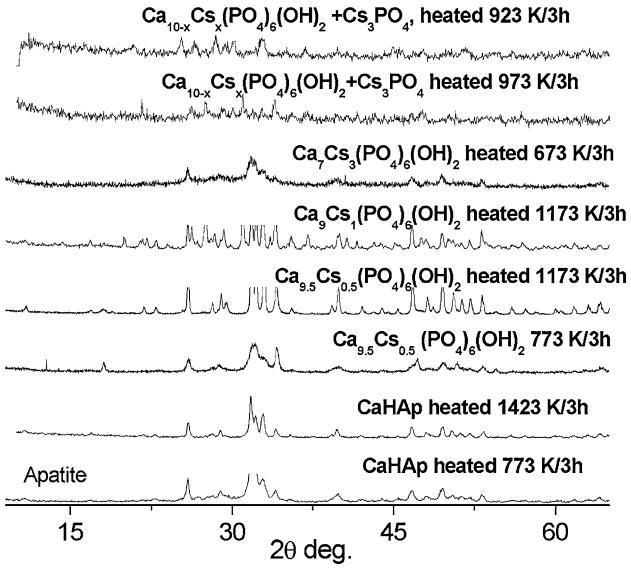

Fig. 4 XRD of $Ca_{10-x}Cs_x(PO_4)_6(OH)_2$ showing phase stability at various temperatures

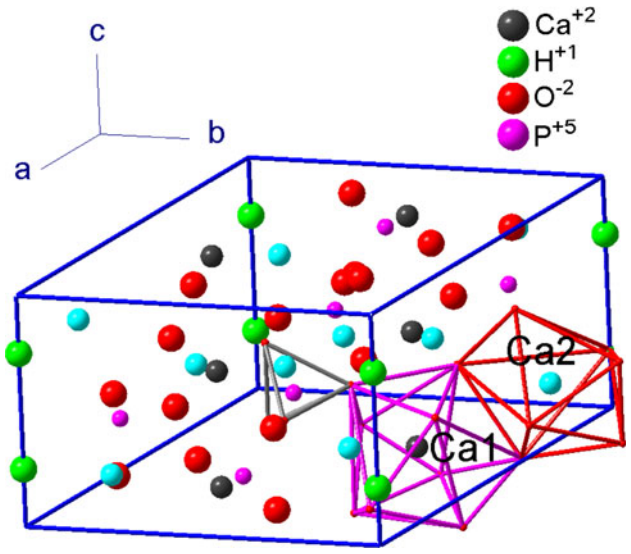

Fig. 5 Schematic of $Ca_{10}(PO_4)_6(OH)_2$ showing Ca_IO_9 and Ca_2O_7 polyhedra

polyhedra are corner shared along *c*-axis, and Ca_IO_9 polyhedra are face shared as shown in Fig. 5. Ca_IO_9 and Ca_{II}-$O_6(OH)$ polyhedra are interconnected by PO_4 tetrahedra. Further, Ca_{II}-$O_6(OH)$ and Ca_IO_9 polyhedra are edge shared.

The lattice parameters of the hexagonal unit cell of CaHAp and Cs-substituted compositions are $a = 9.435(2)$ Å, $c = 6.887(2)$ Å, and $a = 9.384(2)$ Å, $c = 6.893(3)$ Å, respectively, at 298 K. The decrease of lattice parameter *a* for the Cs-doped composition is ascribed to the partial removal of OH^- from Ca_{II}-$O_6(OH)$ polyhedra and creation of OH^- vacancies $\left(r^{VI}_{OH^-} = 1.37 \text{ Å}\right)$ (Ref 19) of the unit cell; the change in the parameter *c* is less significant, perhaps due to the presence of the rigid face-shared columns of polyhedra along the *c*-axis as shown in Fig. 5.

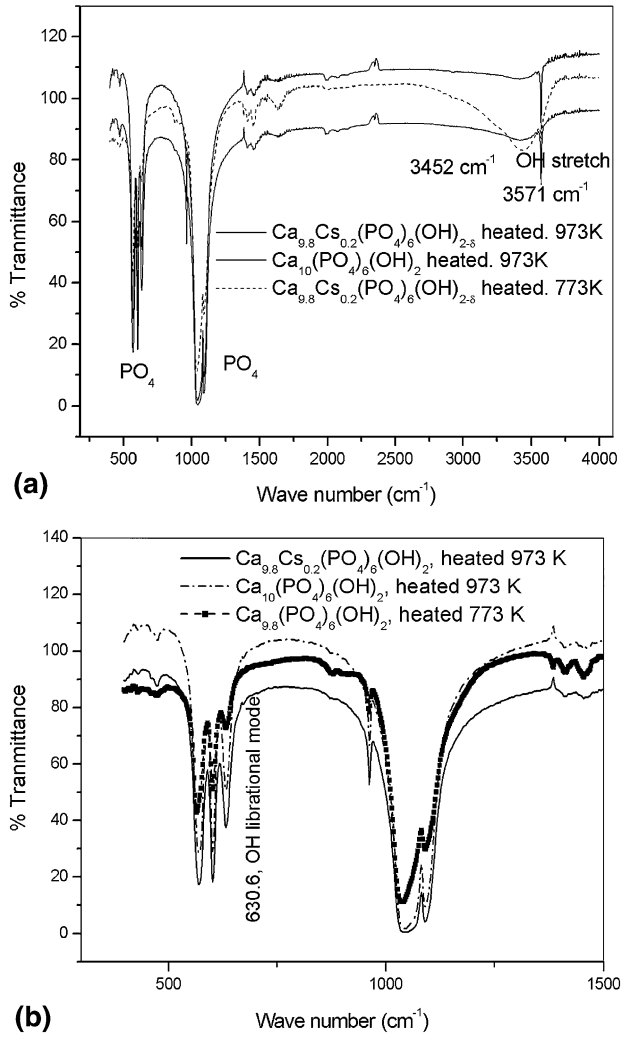

Fig. 6 (a) FTIR spectra of $Ca_{10-x}Cs_x(PO_4)_6(OH)_{2-\delta}$, $x = 0$-0.2, $\delta = 0$-0.04. (b) FTIR spectra of $Ca_{10-x}Cs_x(PO_4)_6(OH)_2$, $x = 0$-0.2 showing OH librational (torsional) mode of vibration

The presence of hydroxyl groups (OH) is indicated by the FTIR spectrum of CaHAp and Cs-substituted CaHAp in Fig. 6(a). $Ca_{9.8}Cs_{0.2}(PO_4)_6(OH)_2$ sample heat-treated at 773 K shows broad OH stretching band at 3452 cm^{-1} corresponds to surface P-OH stretching and a sharp band at 3571 cm^{-1} which corresponds to the lattice OH^- stretching. Figure 6(b) shows the librational (torsional) mode of lattice OH^- which is characteristic of lattice hydroxyls and differentiates from the surface adsorbed hydroxyls. These observations agree well with the literature data (Ref 20, 21). $Ca_{9.78}Cs_{0.2}(PO_4)_6(OH)_{1.96}$ sample heated at 973 K shows only the stretching modes of lattice hydroxyls (3571 cm^{-1}). This indicates a proportionate loss of hydroxyl ions on substitution of Cs at the Ca-site in CaHAp lattice leading to the formation of hydroxyl defects. This was also further supported by TG-DTA experiments of the samples.

3.2 High-Temperature Thermal Expansion

The HTXRD patterns recorded in situ at various temperatures is shown in Fig. 7 for $Ca_{9.8}Cs_{0.2}(PO_4)_6(OH)_2$. These patterns indicate the phase stability and phase purity of the 2 mol% Cs-substituted composition. Variation of lattice

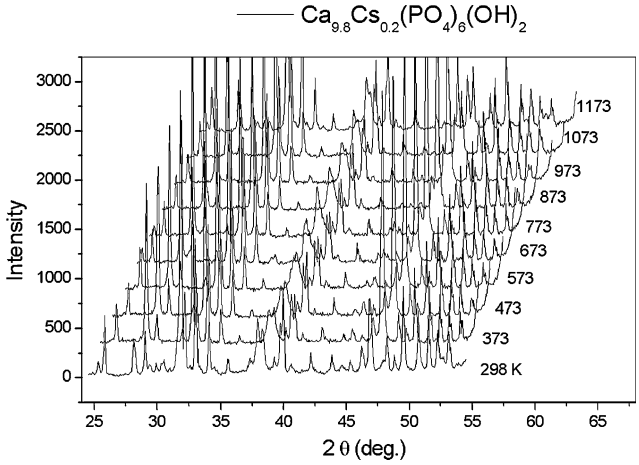

Fig. 7 High-temperature XRD patterns of $Ca_{9.8}Cs_{0.2}(PO_4)_6(OH)_{2-\delta}$

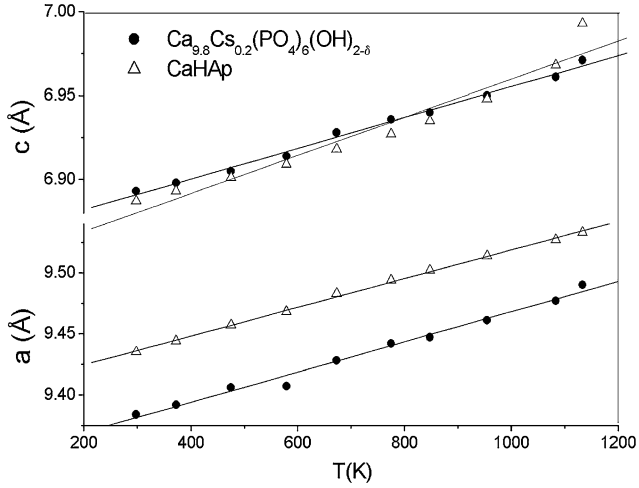

Fig. 8 Lattice parameter variations as function of temperature of CaHAp and $Ca_{9.78}Cs_{0.2}(PO_4)_6(OH)_{2-\delta}$

parameters *a* and *c* with temperature is shown in Fig. 8. The lattice parameters are found to increase linearly with temperature. The coefficient of average linear thermal expansion between room temperature and 1083 K are $\alpha_a = 12.42 \times 10$ 6 K^{-1}, $\alpha_c = 14.98 \times 10^{-6}$ K^{-1}; and $\alpha_a = 12.62 \times 10^{-6}$ K^{-1}, $\alpha_c = 12.57 \times 10^{-6}$ K^{-1} for CaHAp and the Cs-substituted material, respectively. On Cs-substitution, the coefficient of linear expansion along the *c*-axis decreased by 2.56×10^{-6} K^{-1} unit. This may be due to the partial removal of OH^- anions and consequent rearrangement of Ca_{II}-$O_6(OH)$ polyhedra along the *c*-axis. It is interesting to note that the thermal expansion behavior of the apapite material has become nearly isotropic upon Cs-substitution. The bulk thermal expansions measured by dilatometry and average linear expansion measured by HTXRD are compared in Fig. 9 for $Ca_{10}(PO_4)_6(OH)_2$ composition. The two are in very good agreement. In Fig. 10, the linear expansion of $Ca_{10}(PO_4)_6(OH)_2$ is the highest among the Cs-substituted compositions. The linear expansion of 2 mol% Cs-substitution is the least. This may be attributed to the formation of proportionate hydroxyl defects on substitution of Cs- at Ca-site in CaHAp. The formation of hydroxyl defects brings down the expansion along *c*-axis.

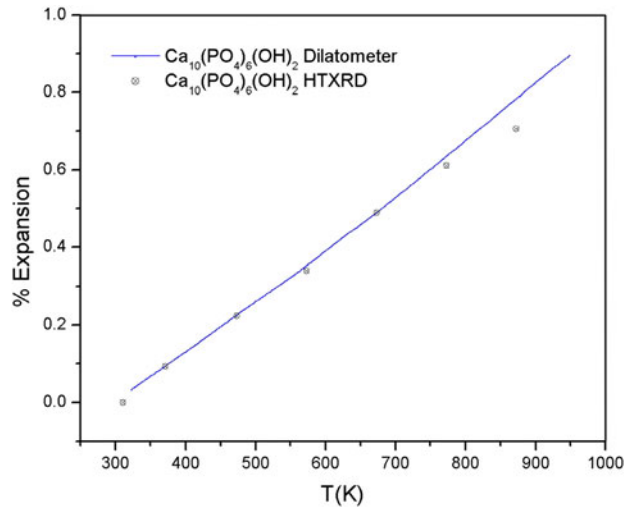

Fig. 9 Percentage linear expansion measured by dilatometry and HTXRD

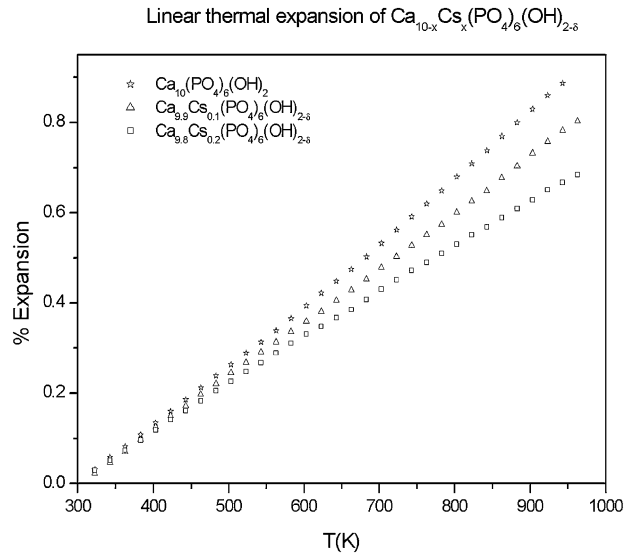

Fig. 10 Percentage linear expansion measured by dilatometry of $Ca_{10-x}Cs_x(PO_4)_6(OH)_{2-\delta}$ (x = 0-0.2, δ = 0-0.04)

4. Conclusions

Cs, 30 mol%, is seen to be loaded into the nanocrystalline apatite matrix. However, high-temperature stability (1173 K) is found to be limited to compositions containing ≤5 mol% Cs. The thermal expansion behavior of the compounds is anisotropic, and the average expansion coefficients are found to be $> 10 \times 10^{-6}$ K^{-1}. The % of thermal expansion measured by HTXRD and dilatometry are in good agreement.

References

1. M. Mathew and S. Tagaki, Structures of Biological Materials in Dental Research, *J. Res. Natl Inst. Stand. Technol.*, 2001, **106**(6), p 1035–1044

2. M. Wei, J.H. Evans, T. Bostrom, and L. Grøndhal, Synthesis and Characterization of Hydroxyapatite, Fluoride-Substituted Hydroxyapatite and Fluorapatite, *J. Mater. Sci. Mater. Med.*, 2003, **14**, p 311–320
3. M.E. Fleet and Y. Pan, Site Preference of Nd in Fluorapatite [$Ca_{10}(PO_4)_6F_2$], *J. Solid State Chem.*, 1994, **112**, p 78–81
4. P. Trocellier, Immobilization of Radionuclides in Single-Phase Crystalline Waste Forms: A Review on Their Intrinsic Properties and Long Term Behaviour, *Ann. Chim. Sci. Mat.*, 2000, **25**, p 321–337
5. J.O. Nriagu, Lead Orthophosphates. IV. Formation and Stability in the Environment, *Geochim. Cosmochim. Acta*, 1974, **38**, p 887–898
6. J.O. Nriagu, Lead Orthophosphates—II. Stability of Cholopyromophite at 25 °C, *Geochim. Cosmochim. Acta*, 1973, **37**, p 367–377
7. J.O. Nriagu, Lead Orthophosphates—III. Stabilities of Fluoropyromorphite and Bromopyromorphite at 25 °C, *Geochim. Cosmochim. Acta*, 1973, **37**, p 1735–1743
8. L.S. Keto and S.B. Jacobsen, Nd and Sr Isotopic Variations of Early Paleozoic Oceans, Earth and Planet, *Sci. Lett.*, 1987, **84**, p 27–41
9. J.L. Conca and J. Wright, An Apatite II, Permeable Reactive Barrier to Remediate Groundwater Containing Zn, Pb and Cd, *Appl. Geochem.*, 2006, **21**, p 1288–1300
10. X. Chen, J.V. Wright, J.L. Conca, and L.M. Peurrung, Effects of pH on Heavy Metal Sorption on Mineral Apatite, *Environ. Sci. Technol.*, 1997, **31**(3), p 624–631
11. M.I. Kay, R.A. Young, and A.S. Posner, Crystal Structure of Hydroxyapatite, *Nature*, 1964, **204**, p 1050–1052
12. A. Chartier, C. Meis, and J.D. Gale, Computational Study of Cs Immobilization in the Apatites $Ca_{10}(PO_4)6F_2$, $Ca_4La_6(SiO_4)6F_2$ and $Ca_2La_8(SiO_4)6O_2$, *Phy. Rev. B*, 2001, **64**, p 9–085110
13. H. Jena, R. Asuvathraman, and K.V.G. Kutty, Phase Stability and Thermal Expansion Studies on Cs-Substituted Nano-Crystalline Ca-Hydroxyapatites Synthesized by Novel Wet Chemical Methods, *Proceedings of 16th National Symposium on Thermal Analysis* (THERMANS-2008), S. Varma et al., Ed., 4-6 Feb, 2008, IGCAR, Kalpakkam, India, p 202–204
14. B.D. Cullity and S.R. Stock, *Elements of X-Ray Diffraction*, 3rd ed., Prentice-Hall Inc, Upper Saddle River, 2001, p 167–171
15. R. Jenkins and R.L. Snyder, *Introduction to X-ray Powder Diffractometry*, Wiley & Sons Inc, New York, 1996, p 89–91
16. K.V. Govindan Kutty, R. Asuvathraman, M.V. Krishnaiah, V. Ganesan, R. Parthasarathy, D. Sai Subalakshmi, B. Suhasini, K.C. Srinivas, K.A Gopal, and P.V. Kumar, *Design, Fabrication and Commissioning of a Push Rod Dilatometer for Thermal Expansion Studies on Solids*, IGC-283, Indira Gandhi Centre for Atomic Research, Kalpakkam, India, 2006
17. H. Jena, Ch.V. Rao, F.P. Eddy, J. Dooley, and B. Rambabu, Structural and Proton Transport Studies on Nano-Crystalline [$Ca_{10}(PO4)_6(OH)_2$] (HAp), HAp-Nafion® Composite, and Natural Human Bbone, *Phys. Status Solidi A*, 2009, **206**(11), p 2536–2541
18. H. Fernandez-Morán and A. Engström, Electron Microscopy and X-ray Diffraction of Bone, *Biochim. Biophys. Acta*, 1957, **23**, p 260–264
19. R.D. Shannon, Revised Effective Ionic Radii and Systematic Studies of Interatomic Distances in Halides and Chalcogenides, *Acta Cryst.*, 1976, **A32**, p 751–767
20. S. Koutsopoulos, Synthesis and Characterization of Hydroxyapatite Crystals: A Review Study on the Analytical Methods, *J. Biomed. Mater. Res.*, 2002, **62**, p 600–612
21. H. Yu, H. Zhang, X. Wang, Z. Gu, X. Li, and F. Deng, Local Structure of Hydroxy Peroxy Apatite: A Combined XRD, FT-IR, Raman, SEM, and Solid State NMR Study, *J. Phys. Chem. Solid*, 2007, **68**(10), p 1863–1871